Phys Chem Minerals (2006) 33: 445–456
DOI 10.1007/s00269-006-0095-9

ORIGINAL PAPER

Siew Wei Goh · Alan N. Buckley · Robert N. Lamb
Liang-Jen Fan · Ling-Yun Jang · Yaw-wen Yang

# Pentlandite sulfur core electron binding energies

Received: 23 March 2006 / Accepted: 11 May 2006 / Published online: 11 July 2006


**Abstract** A number of freshly abraded surfaces of pentlandite have been characterised by X-ray photoelectron spectroscopy to establish whether the initial intensity of the S 2*p* component near 161.4 eV, previously assigned to the 25% of S atoms in fourfold coordination by metal atoms in pentlandite, was always at least 25% of the total S 2*p* intensity. It was found that the intensity of this S 2*p* component could be lower than 20% for surfaces that were not significantly oxidised. To assess whether the proposed 0.75–0.8 eV 2*p* binding energy difference for the two sulfur environments in pentlandite was justified, ab initio calculations of the difference in core electron binding energies and of the densities of unfilled states have been carried out. The corresponding simulated S K near-edge X-ray absorption fine structure (NEXAFS) spectra have been compared with experimental spectra. The calculated S 2*p* and S 1*s* binding energy differences were 0.45 and 0.5 eV at most, in agreement with the experimental NEXAFS spectra. It was concluded that the S 2*p* component near 161.4 eV arises entirely from violarite present at the pentlandite surface rather than from 4-coordinate S in pentlandite itself. Ab initio calculations of the difference in S 2*p* binding energies for the 2- and 3-coordinate S in stibnite have also been carried out and found to be quite small, in agreement with previously reported experimental values. Nevertheless, for both pentlandite and stibnite, calculations have confirmed that an increase in coordination number is associated with an increase in sulfur core electron binding energies, even although that increase is barely measurable for the latter sulfide.

S. W. Goh · A. N. Buckley (✉) · R. N. Lamb
Surface Science and Technology, School of Chemistry,
University of New South Wales, Sydney, NSW 2052, Australia
E-mail: a.buckley@unsw.edu.au
Tel.: +61-2-93854645
Fax: +61-2-96621697

L.-J. Fan · L.-Y. Jang · Y. Yang
National Synchrotron Radiation Research Center,
Hsinchu Science Park, Hsinchu 30076, Taiwan

**Keywords** Pentlandite · XPS · NEXAFS · Ab initio calculations · Stibnite

## Introduction

Pentlandite, $(Fe,Ni,Co)_{9\pm x}S_8$, is difficult to investigate by means of spectroscopic techniques because naturally-occurring specimens of the mineral are often intimately associated with its supergene alteration product violarite, ideally $FeNi_2S_4$ but of general composition $(Fe,Ni)_3S_4$ (Misra and Fleet 1974). Moreover, pentlandite usually occurs as intergrowths with pyrrhotite (Francis et al. 1976). In particular, the study of pentlandite by using X-ray photoelectron spectroscopy (XPS) to characterise fracture surfaces has been unsatisfactory because cleavage appears to take place typically along an interface with an altered phase (Buckley and Woods 1991a; Legrand et al. 1997). Surfaces prepared by abrasion have proved superior in this regard, but whereas fracture surfaces can be prepared under ultra high vacuum, it is difficult to prepare swarf-free abraded surfaces in the total absence of residual oxygen, and hence without the possibility of some surface oxidation.

The lower binding energy region of the S 2*p* spectrum from an abraded or fracture surface of pentlandite can be fitted adequately with two unresolved doublet components at $2p_{3/2}$ binding energies near 161.4 and 162.2 eV, with the latter component usually being significantly more intense than the former. Buckley and Woods (1991a) concluded that the 162.2 eV component arose from unaltered pentlandite, and the component at 161.4 eV was due to a violarite-like altered phase, in broad agreement with the findings of Richardson and Vaughan (1989). However, Legrand et al. (1997) obtained a fracture surface from pentlandite, entirely surrounded by millerite, that appeared to be largely unoxidised notwithstanding the observation of a relatively intense O 1*s* peak from the same surface, and assigned both 2*p* doublets in the S 2*p* spectrum from that surface to unaltered pentlandite. The O 1*s* peak was

attributed predominantly to water. The lower binding energy S 2*p* component was assigned to the 25% of S atoms in 4-coordinate metal atom environments and the higher binding energy component to the 75% of S atoms in 5-coordinate environments. The intensity ratio they observed was 1.2:3, close to the expected ratio of 1:3. More recently, Legrand et al. (2005) observed an intensity ratio of 8:3 (2.7:1) from a freshly abraded surface, and rationalised the much higher than expected component near 161.3 eV in that particular S 2*p* spectrum as having arisen from violarite in addition to the pentlandite 4-coordinate S.

The interpretation of the pentlandite S 2*p* spectrum proposed by Legrand et al. (1997, 2005) appeared to be a reasonable one. Nevertheless, it is of some concern that the relative intensity of the lower binding energy component can vary markedly for different surfaces prepared by fracture or abrasion, especially as the intensity of that component changes comparatively slowly on subsequent exposure of the surface to air (Buckley and Woods 1991a). It is possible that the S 2*p* binding energy for the 4-coordinate S in pentlandite is very similar to that for the (4-coordinate) S in violarite. It is also possible that the S atoms in pentlandite have 2*p* binding energies that differ by significantly less than 0.8 eV, and that essentially all of the lower binding energy component arises from violarite or a related sulfide phase. In that case, the surface concentration of violarite at the fracture surface examined by Legrand et al. (1997) would have been fortuitously close to 25%. An appreciable difference in binding energy for the two S coordination environments in pentlandite is not a foregone conclusion, as it has been shown that there is no necessary relationship between core electron binding energies and coordination for S atoms in Ni sulfides (Goh et al. 2006a), and the S 2*p* binding energies for the 2- and 3-coordinate S in stibnite ($Sb_2S_3$) have been shown to differ by 0.4 eV at most (Zakaznova-Herzog et al. 2006). On the other hand, to date there are no known reports of pentlandite S 2*p* spectra for which the intensity of the lower binding energy component is less than 28%.

In order to assess the validity of the assignment of the S 2*p* spectrum for pentlandite in terms of a binding energy difference of ~0.8 eV for the two S environments in that mineral, a number of abraded surfaces of pentlandite have been characterised by XPS to establish whether the initial intensity of the lower binding energy S 2*p* component was always at least as great as 25%. Photoelectron spectra after prolonged exposure of the abraded surfaces to air were also obtained. In addition, to determine whether a binding energy difference as large as ~0.8 eV for the two S environments might be justified, ab initio calculations of the difference in core electron binding energies and of the densities of unfilled states have been carried out. The corresponding simulated S K near-edge X-ray absorption fine structure (NEXAFS) spectra have been compared with experimental spectra to gauge the accuracy of the calculated densities of states and core electron binding energy differences. To further assess both the ability of ab initio calculations to correctly estimate S core electron binding energies, and the validity of the previously postulated relationship between S coordination and core electron binding energies, S 2*p* binding energies for stibnite have been calculated and compared with recently reported experimental values (Zakaznova-Herzog et al. 2006).

## Experimental and computational details

A low Co pentlandite from Kambalda, Western Australia was investigated. Based on electron microprobe analysis, the mineral was Ni-rich, with a composition $Ni_{4.7}Fe_{4.25}Co_{0.05}S_8$. SEM analysis revealed some small inclusions of chalcopyrite and pyrrhotite but no pyrite. However, no Cu peaks were observed in the photoelectron spectra, eliminating the possibility that inclusions of chalcopyrite contributed to the S 2*p* spectra discussed. The heazlewoodite ($Ni_3S_2$) used as a reference material in this study was synthesised by treating a sintered compact of Ni powder in a 4:1 $H_2/H_2S$ atmosphere at 380°C. A dense, coherent ~2 mm thick layer of the sulfide was produced on the surface of the Ni metal, and XRD and electron microprobe analyses confirmed that this layer had the heazlewoodite structure (Buckley and Woods 1991b). Each pentlandite or heazlewoodite surface to be examined was abraded in air while wet with propan-2-ol before being transferred as quickly as possible to the insertion chamber of the photoelectron spectrometer or soft X-ray beam-line end-station.

Conventional monochromatised Al $K_\alpha$ XPS analyses were carried out on a VG ESCALAB 220-iXL spectrometer. An analyser pass energy of 20 eV and an electron take-off angle of 90° were used. Included in the binding energies used for calibration were 932.67 eV and 83.96 eV for Cu $2p_{3/2}$ and Au $4f_{7/2}$ from metallic copper and gold, respectively.

S 2*p* spectra were fitted with the VG Eclipse, CasaXPS and XPSPEAK 4.1 (Kwok 2000) programs assuming a Shirley background. When symmetric Gaussian-Lorentzian lineshapes were used, the additional doublet to account for the high binding energy region of the spectrum was restricted to a binding energy no lower than 163 eV and a linewidth of no more than 2 eV. The $2p_{1/2}$ and $2p_{3/2}$ components were assigned equal linewidths, an energy separation of 1.19 eV and an intensity ratio of 1:2. In the fitting of the S 2*p* spectrum from an oxidised surface with doublets from the 5-coordinate S in pentlandite and from violarite, the linewidths were not constrained to be the same. Similarly, in the fitting of the spectrum from a briefly air-exposed surface with a doublet from the 5-coordinate S in pentlandite, a doublet of one-third the intensity of, and the same linewidth as, the principal component from the 4-coordinate S, and a doublet from violarite at a binding energy 0.85 eV lower than that for the principal component, the linewidths of the components from the two phases were not constrained to be the same.

Lineshapes with Lorentzian proportion varying from 30 to 50% were used, with 40% giving the best fit to the low binding energy edge.

The NEXAFS spectra were determined in a UHV end-station on the bending magnet beam-line 15B at the NSRRC in Hsinchu. Each specimen was held in place on the manipulator sample holder by stainless steel screws. Both total electron and total fluorescence yield S K-edge spectra were determined using a Kohzu double Si(111) crystal monochromator, which provided a resolution at that edge of ~0.4 eV. The photon flux incident on the specimen, $I_0$, was monitored by a proportional counter incorporating He gas contained between two 75 μm Be windows. Spectra shown have been normalised ($I/I_0$). Pyrite was used for energy calibration; the initial (white line) S K-edge peak maximum was taken to be 2471.3 eV, as that value had been determined relative to the corresponding peak for elemental sulfur at 2472.0 eV (Li et al. 1995).

Ab initio calculations were carried out using the FEFF8 (Ankudinov et al. 1998, 2002) and WIEN2k (Blaha et al. 1990; Schwarz et al. 2002) codes. For the FEFF8 calculations, potentials were calculated self consistently within a 0.7 nm radius cluster (about 100 atoms) around the absorbing S atom with 15% overlap of the muffin-tin radii. Calculations using the partially non-local Dirac-Fock/Hedin-Lundqvist potential were carried out for both an unscreened and a fully screened core hole with full multiple scattering up to $l = 2$ with cluster radii of at least 1 nm, equivalent to about 450 atoms. With an unscreened core hole, the relative intensity and position of the leading absorption peak in a simulated spectrum were lower (typically by ~10% and ~0.5 eV, respectively, for S K-edge absorption) than for a fully screened core hole. The form of an experimental spectrum was usually between those of the corresponding spectra simulated with an unscreened or a fully screened core hole. The input files were generated by the program ATOMS via the graphical interface TkATOMS (Ravel 2001). For the WIEN2k calculations, the unit cell parameters were entered into the structure generation subroutine. For both codes, the crystallographic structure data used in the calculations were those reported by Pearson and Buerger (1956) and Rajamani and Prewitt (1973) for Ni, Fe pentlandite, by Chauke et al. (2002) for Co pentlandite, by Fleet (1977) for heazlewoodite, and by Kyono et al. (2002) for stibnite.

## Results and discussion

### X-ray photoelectron spectra of freshly abraded pentlandite surfaces

The photoelectron spectra from all the freshly abraded pentlandite surfaces examined in this investigation displayed peaks from carbon and oxygen. At least some of that carbon and oxygen would have arisen from contamination during the abrasion, but some could also have been due to the presence of weathered mineral within the depth analysed and/or the products of pentlandite that had become oxidised during surface preparation. It was clear that the concentration of oxygen-containing species was significantly lower at some surfaces than at others, notwithstanding the similar preparation procedure. The Ni 2*p*, Fe 2*p* and O 1*s* spectra from a surface for which the O 1*s* intensity was relatively low (Fig. 1a), indicated that at least a small proportion of the oxygen was associated with pentlandite oxidation

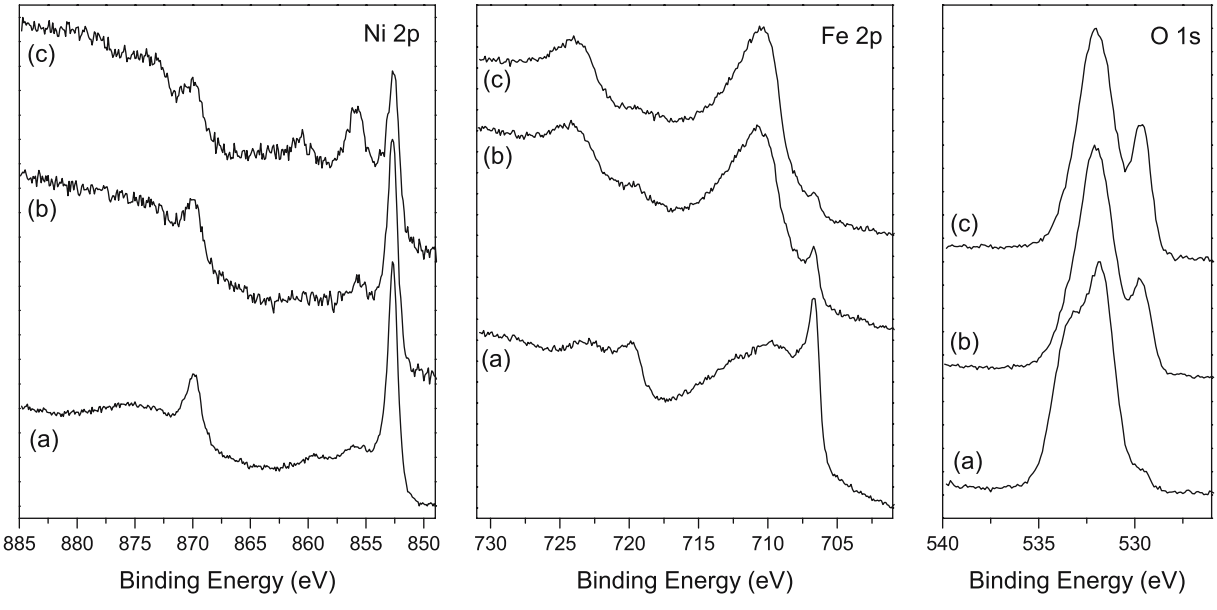


**Fig. 1** Ni 2*p*, Fe 2*p* and O 1*s* spectra from the same abraded pentlandite surface exposed to air for: **a** less than 1 min; **b** 68 h; **c** 782 h

products. The small O 1*s* peak near 529.9 eV would almost certainly have arisen from Ni or Fe oxide, but the significantly more intense peak above 533 eV would have been due to physisorbed water. Assignment of the O 1*s* peak near 532 eV is less straightforward, as chemisorbed water and hydrated Ni or Fe oxides are possible sources (Knipe et al. 1995; Legrand et al. 1997). The low intensity peak near 856 eV in the corresponding Ni 2*p* spectrum is consistent with the presence of a small concentration of Ni-oxygen species, while the main $2p_{3/2}$ peak at 852.6 eV is at the binding energy previously observed for pentlandite (Buckley and Woods 1991a; Legrand et al. 1997). The main $2p_{3/2}$ peak at 706.8 eV in the Fe 2*p* spectrum is also at the binding energy expected for pentlandite, but a broad contribution in the range 709–711 eV would have arisen from Fe-oxygen species (Buckley and Woods 1991a; Legrand et al. 1997). The poorly-resolved peak at 712.6 eV can be assigned to Ni LMM Auger electrons (Legrand et al. 1997). An apparently greater concentration of Fe–O than Ni–O species is quite consistent with the initial oxidation of the pentlandite (vide infra). Thus, the O 1*s*, Ni 2*p* and Fe 2*p* spectra in Fig. 1a all indicate a small degree of oxidation of the surface, as did the corresponding spectra obtained by Legrand et al. (1997) for their fracture surface.

The S 2*p* spectrum (Fig. 2a) corresponding to the spectra shown in Fig. 1a for a freshly abraded surface consists predominantly of a doublet at a $2p_{3/2}$ binding energy of 162.2 eV with a shoulder just discernible near 161.4 eV. The spectrum in Fig. 2a is similar to the spectrum reported by Legrand et al. (1997), except that the shoulder in Fig. 2a is slightly less evident, and the overall width of the spectrum at half height is ~5% smaller. It is the origin of the incipient shoulder near 161.4 eV that is the crux of the issue being addressed in this paper.

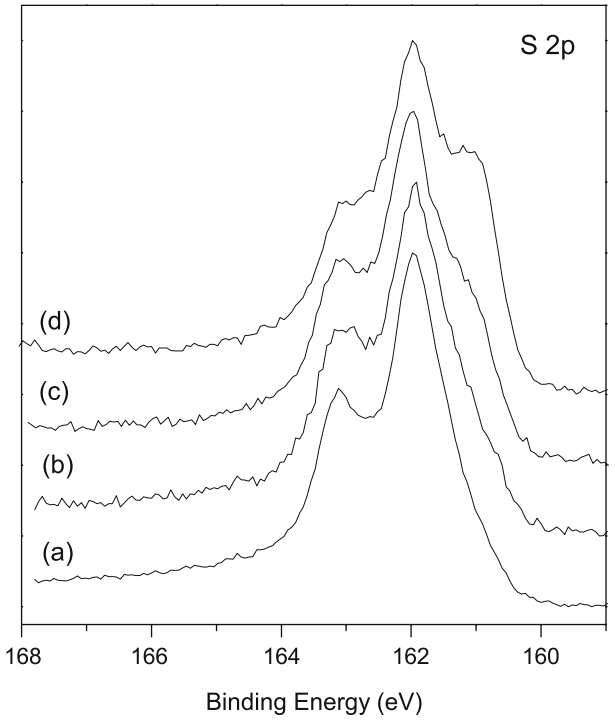


**Fig. 2** S 2*p* spectrum from the same abraded pentlandite surface exposed to air for: **a** less than 1 min; **b** 1 h; **c** 68 h; **d** 782 h

## X-ray photoelectron spectra of pentlandite surfaces exposed to air

The same pentlandite surface from which the spectra in Figs. 1a and 2a were obtained, was exposed to air under ambient conditions for up to 32 days, with Ni 2*p*, Fe 2*p*, O 1*s* and S 2*p* spectra determined at various stages throughout that period. Spectra obtained after exposure of the surface for 68 h are shown in Figs. 1b and 2c, and those after exposure for 782 h are shown in Figs. 1c and 2d. The S 2*p* spectrum after exposure for 1 h is shown in Fig. 2b.

It can be seen from Fig. 1 that with increasing exposure to air, the concentration of Ni-oxygen species in the surface layer increases moderately, the concentration of Fe-oxygen species increases markedly, and the relative intensity of the 529.9 eV O 1*s* component attributed to unhydrated oxide increases noticeably. It is evident from the deteriorating signal/noise ratio of the Ni 2*p* spectra in Fig. 1b and c (which had a similar total scan time as that in Fig. 1a) that the Ni remaining in the sulfide lattice becomes decreasingly represented in the depth analysed. The relative intensity of the S 2*p* spectra too decreased with increasing exposure time, but this is not obvious from Fig. 2 as the total scan time was increased and the S 2*p* analysis depth is greater than that for the Ni 2*p*. Also not evident from Fig. 2 because of the limited binding energy range shown is the absence of peaks from sulfate or other S-oxygen species even for the longest exposure time. What is clear from Fig. 2 is that the relative intensity of the component near 161.4 eV increases with exposure time, and curve fitting reveals that the increase is in fact asymptotic for extended

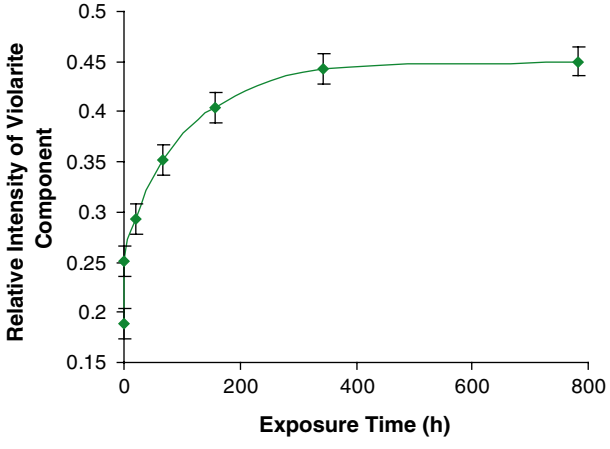


**Fig. 3** Intensity of violarite component relative to that of total S 2*p* spectrum as a function of exposure time of surface to air

exposure (Fig. 3). These observations are in broad agreement with previous studies (Buckley and Woods 1991a; Legrand et al. 1997) and are consistent with the oxidation of pentlandite to a thiospinel such as violarite with the concomitant formation of metal–oxygen species that cover the violarite layer. It should be noted that even if a small part of the intensity in the 161–162 eV binding energy region had been due to minor inclusions of pyrrhotite, which has a S $2p_{3/2}$ binding energy near 161.2 eV, that intensity would have decreased rather than increased on oxidation (Buckley and Woods 1985).

The notional reaction for the oxidation of pentlandite in air under ambient conditions:

$$8Fe_{4.5}Ni_{4.5}S_8 + 17O_2 \rightarrow 16FeNi_2S_4 + 10Fe_2O_3 + 4NiO \quad (1)$$

is consistent with the photoelectron spectra, in that the surface concentration of oxidised Fe is significantly greater than that of oxidised Ni (notwithstanding the slightly greater surface sensitivity of Ni 2*p* compared with Fe 2*p* photoelectrons). However, as noted above, $FeNi_2S_4$ is no more than an ideal representation of violarites, and the stoichiometry of the phase actually produced could be somewhat different while still being within the general composition $(Fe,Ni)_3S_4$. At least some of the Fe and Ni oxides produced would most probably be hydrated; i.e. present as FeOOH and $Ni(OH)_2$. Of particular importance for the issue being addressed is the S $2p_{3/2}$ binding energy of the violarite formed. After extended exposure to air, the $2p_{3/2}$ binding energy for that species can be determined by curve fitting (Fig. 4) to be 0.85 eV below that for the 5-coordinate S in pentlandite; i.e. 161.35 eV relative to 162.2 eV for pentlandite, close to the 161.4 eV determined by Buckley and Woods (1991a). The binding energy is slightly lower than the 161.44 eV obtained for a fracture surface not exposed to air by Legrand et al. (1997) and assigned to 4-coordinate S in pentlandite.

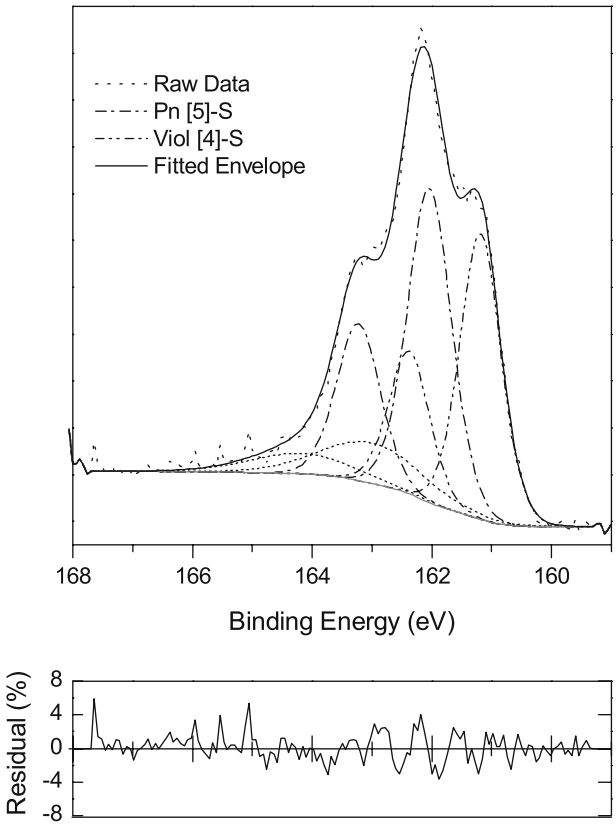


**Fig. 4** S 2*p* spectrum from pentlandite surface exposed to air for 782 h fitted in the low binding energy region with doublets from unaltered pentlandite and violarite (residual also shown)

## Interpretation of the S 2*p* spectrum from a relatively unoxidised pentlandite surface

It is possible to force an approximate fit to the S 2*p* spectrum in Fig. 2a on the same basis as that obtained by Legrand et al. (1997), namely with a principal doublet near 162.2 eV assigned to the 5-coordinate S in pentlandite, a secondary doublet near 161.4 eV attributed to 4-coordinate S, and low intensity components at binding energies above 163 eV to account for S-rich environments such as oligosulfides (or to compensate for the use of a symmetric lineshape). However, such an approximate fit, forced by constraining the intensity ratio of the doublets from 4- and 5-coordinate S to be 1:3, and which results in $2p_{3/2}$ binding energies of 161.35 and 162.1 eV, respectively, is poor on the key low binding energy edge of the spectrum (Fig. 5a). An unconstrained intensity ratio results in a better fit, with the intensity of the doublet from 4-coordinate S being no more than 25% of the intensity of the doublet near 162.2 eV (equivalent to 20% of the sum) (Fig. 5b). In both cases, the linewidth for the two doublets was constrained to be the same. In the latter fit, the 25% intensity of the lower binding energy component is in contrast to the 40% reported by Legrand et al. (1997) and the 33% expected if it indeed arose from 4-coordinate S in pentlandite.

Because of the metallic conductivity of pentlandite, its S 2*p* component lineshape is expected to be asymmetric, and Legrand et al. (1997) reported that they were also able to fit their S 2*p* spectrum with two asymmetric doublets at $2p_{3/2}$ binding energies of 161.44 and 162.19 eV. However, they noted no effect on the fitted intensity ratio of these two doublets resulting from the use of an asymmetric lineshape, and only a minor effect has been observed in the present work. Fits to the higher binding energy region of the S 2*p* spectra obtained in the present work were not as good when asymmetric lineshapes were used.

Legrand et al. (2005) explained the much higher than expected component near 161.3 eV from a freshly abraded pentlandite surface by proposing that the S 2*p* binding energy for violarite was essentially the same as that for the 4-coordinate S in pentlandite. However, it would appear from the poor fit in Fig. 5a and the fitted intensities in Fig. 5b that this proposal is probably not

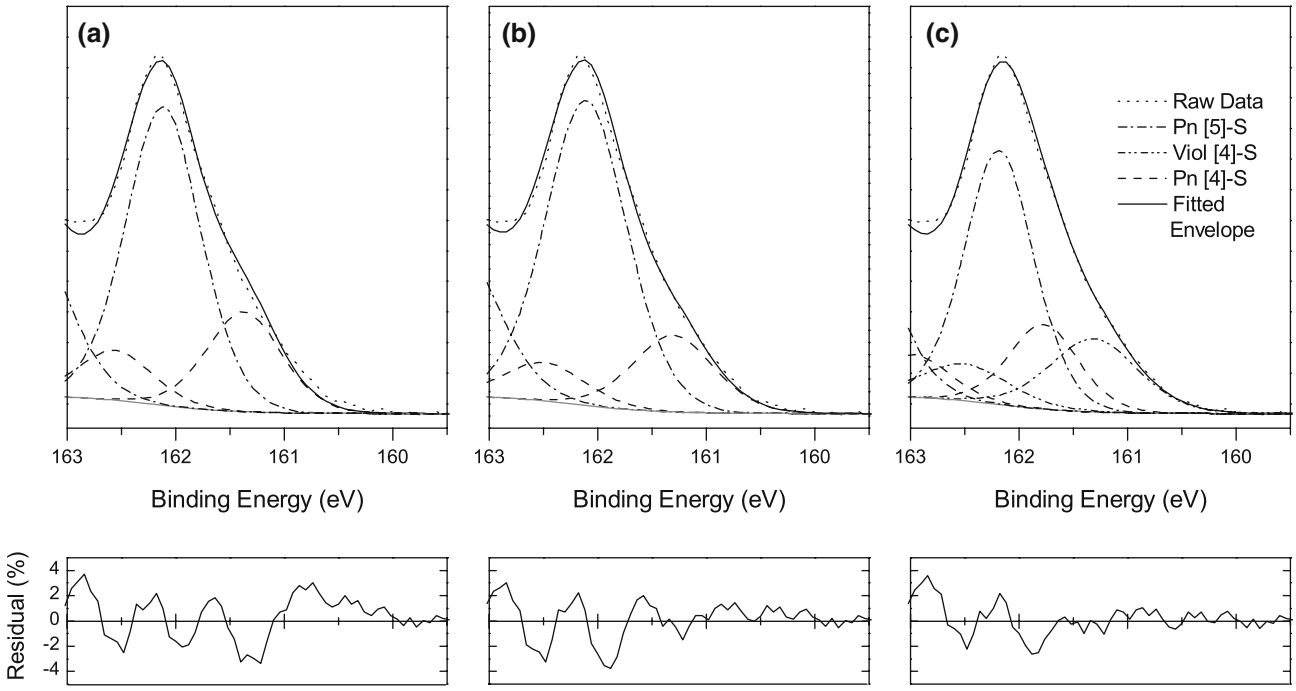


**Fig. 5** Low binding energy region of the S 2*p* spectrum from pentlandite surface exposed to air for less than 1 min fitted with doublets from: **a** 5- and 4-coordinate S in pentlandite with intensity ratio constrained to 3:1; **b** 5- and 4-coordinate S in pentlandite with unconstrained intensity ratio; **c** 5- and 4-coordinate S in pentlandite and violarite

tenable. Nevertheless, this does not necessarily mean that the 4-coordinate S in pentlandite does not have a lower binding energy than that for the 5-coordinate S, but it does mean that the binding energy difference is likely to be significantly less than 0.8 eV.

In order to estimate the binding energy for the 4-coordinate S in pentlandite from the S 2*p* spectrum for a slightly oxidised surface (Fig. 2a), the low binding energy region has to be fitted with three S 2*p* doublets; one near 162.2 eV from the 5-coordinate S, another of one-third the intensity at a binding energy between 162.2 and 161.4 eV from the 4-coordinate S in pentlandite, and one at 161.35 eV from the 4-coordinate S in the violarite present. It was expected that the precise binding energy obtained for the intermediate peak would depend on the parameters and constraints used in the fitting (summarised in the experimental details section) and for this reason, several different fitting routines were used to allow access to different lineshapes. Nonetheless, regardless of the routine or precise lineshape used, the fitted intermediate doublet had a binding energy no more than 0.45 eV lower than that for the 5-coordinate S. One such fitting is shown in Fig. 5c, and the corresponding fitted parameters listed in Table 1. Notwithstanding the essentially invariant fitted binding energy for the doublet corresponding to the 4-coordinate S in pentlandite, this result alone does not represent unequivocal confirmation that the 2*p* binding energy difference for the 4- and 5-coordinate S in pentlandite must be as large as 0.4 eV or less than 0.5 eV.

**Table 1** S 2*p* doublet parameters for the fit shown in Fig. 5c

| Doublet assignment | $2p_{3/2}$ binding energy (eV) | Linewidth (eV) | Lineshape (% Gaussian) |
|---|---|---|---|
| [5]-S in pentlandite | 162.2 | 0.75 | 60 |
| [4]-S in pentlandite | 161.8 | 0.75 | 60 |
| S in violarite | 161.35 | 0.97 | 60 |
| S-rich surface | 163.5 | 2.0 | 60 |

## Experimental NEXAFS spectra

In principle, it should be possible to corroborate the S 2*p* binding energy difference deduced from the fitted S 2*p* photoelectron spectrum by means of experimental and simulated NEXAFS spectra. Corroboration should be feasible at both the S K- and L-edges provided a sufficiently high photon energy resolution were available and provided the absorption linewidth were sufficiently narrow. The core-hole lifetime broadening for the S K-, $L_1$- and $L_{2,3}$-level has been calculated to be 0.59, 1.49 and 0.05 eV, respectively, (Krause and Oliver 1979) therefore absorption at the $L_1$ edge is unlikely to be informative. Although an absorption edge energy depends on both the relevant core electron binding energy and the energy of an appropriate unfilled state, in the case of two environments within a single material of metallic conductivity, the absorption energy difference would predominantly reflect the binding energy difference. This is illustrated in the next section when the

densities of states for the two environments are calculated. One advantage of X-ray absorption spectroscopy (XAS) at the S K-edge, especially if absorption is determined in fluorescence yield mode, is the lower surface sensitivity compared with that at the L-edge or even for S 2*p* photoelectrons excited by less than 1.5 keV photons. Hence, minor oxidation should not confound the K-edge data provided the violarite is present at the surface rather than at weathered interfaces within the mineral. The magnitude of a S 1*s* binding energy difference is $\sim 1.2 \times$ the corresponding S 2*p* difference (Sodhi and Cavell 1986; Chassé et al. 1993), so that a S 1*s* binding energy difference of ~1 eV would be expected if the S 2*p* difference were 0.8 eV.

The S K-edge absorption spectrum for pentlandite is shown in Fig. 6a, with the spectrum for heazlewoodite obtained under the same experimental conditions shown in Fig. 6b for comparison. It is immediately obvious that the leading absorption peak in the pentlandite spectrum is broader than that for $Ni_3S_2$, but still symmetrical. One possible reason for the greater broadening is a significant difference in the core electron binding energies for the two S environments in pentlandite, however, because only 25% of the S atoms would have the lower binding energy, a large binding energy difference would give rise to a noticeable asymmetry or even shoulder at the absorption edge. Another possible reason is a distribution of environments for S atoms in 4- or 5-coordination arising from a mostly random distribution of Ni, Fe and Co atoms in the metal sites. Mössbauer spectroscopic measurements have established that there is a slight preference for Fe atoms to occupy octahedral sites (Knop et al. 1970; Vaughan and Ridout 1971), but otherwise it is expected that metal atom distribution would be random. If this second reason were to be applicable, there should be some evidence to support it in the S 2*p* linewidth. The fitted linewidth of 0.75 eV (Table 1) is slightly broader than that (~0.70 eV) fitted to the S 2*p* spectrum for $Ni_3S_2$ determined under the same experimental conditions, therefore metal atom distribution is likely to have contributed to the broadening of the absorption peaks, but not to have been the sole cause. A third possible reason is a significantly broader energy distribution of the unfilled S *p*-states immediately above the Fermi level for pentlandite compared with heazlewoodite, and this possibility is considered in a subsequent section.

Because the leading S K-edge absorption peak for pentlandite is symmetrical, fitting with two components of equal width and of intensity ratio 1:3 but at different energies can only be effected if the maximum linewidth is constrained or if a minimum separation is specified. Forcing fits on the basis of such constraints indicated that an energy separation of no more than 0.6 eV would be possible, as a separation of even this value resulted in a noticeable asymmetry or incipient shoulder on the absorption edge (the low energy side of the fitted absorption peak). Thus, the XAS data suggest a S 1*s* binding energy difference of no more than 0.6 eV, equivalent to a S 2*p* binding energy difference no greater than 0.5 eV. Although this finding corroborates that from the fitting of the S 2*p* spectra, it is still insufficient to constitute unambiguous confirmation that the 4- and 5-coordinate S 2*p* binding energy difference must be as large as 0.4 eV or can be no greater than 0.5 eV, as the linewidth (1.55 eV) for the two components fitted to the pentlandite S K-edge absorption peak was greater than that for the heazlewoodite absorption peak shown in Fig. 6b. Therefore, additional evidence is necessary, such as that from a theoretical estimation of the core electron binding energy difference. Estimation of the binding energy difference is an integral part of any

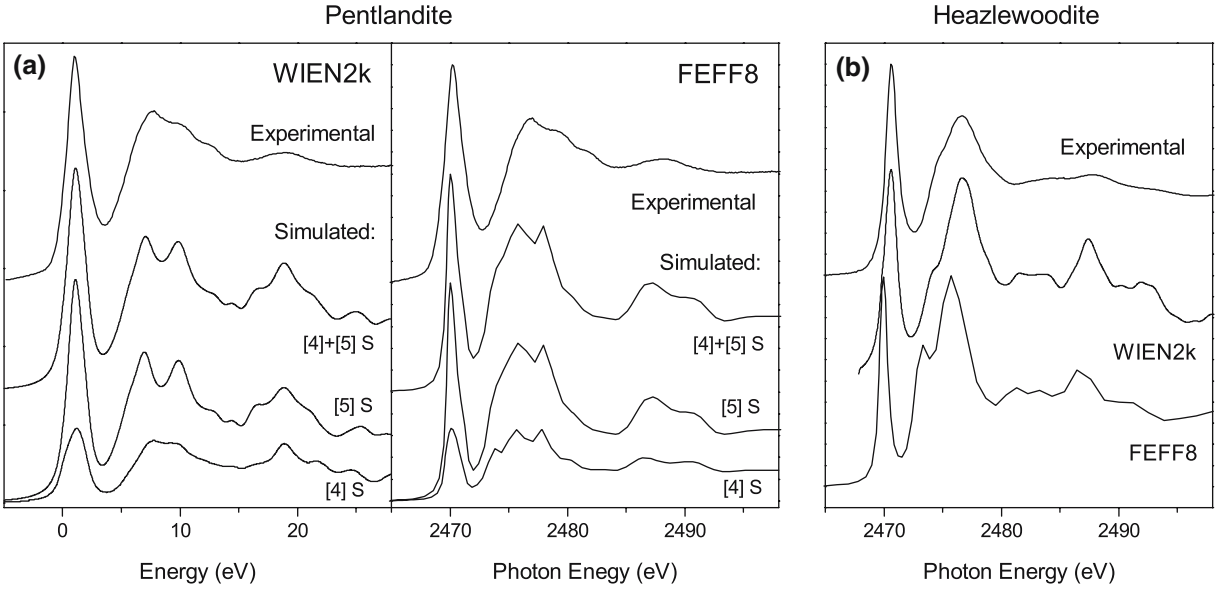


**Fig. 6** S K-edge NEXAFS spectrum, and spectra simulated using FEFF8 and WIEN2k for: **a** pentlandite; **b** heazlewoodite

simulation of the sulfur NEXAFS spectra for pentlandite via codes such as FEFF8 or WIEN2k.

## Calculated sulfur core electron binding energies

Previous attempts to calculate core electron binding energies using FEFF8 have provided absolute values much closer to those determined experimentally by XPS than expected (Goh et al. 2006a), but binding energy differences that moderately underestimate observed values (Goh et al. 2006b). By contrast, while default absolute binding energies determined using WIEN2k were typically underestimated quite markedly, binding energy differences for different sites in the same lattice appear to agree well with experimentally determined values (Goh et al. 2006b). Energies are calculated for all atomic levels at the same time in WIEN2k relative to exactly the same Fermi level, whereas a separate FEFF8 calculation is required for each level. Accordingly, greater weight should be given to the core electron binding energy differences for the S atoms in pentlandite estimated by WIEN2k than by FEFF8.

Calculating the electronic properties of a synthetic pentlandite such as $Co_9S_8$ is computationally demanding but relatively straightforward as the same metal (Co) is present in all 36 metal sites in the crystal structure. However, calculations for natural pentlandites are complicated because either Ni or Fe atoms can occupy each of the 32 tetrahedral and 4 octahedral metal sites. The input file for both ab initio codes has to be adapted to accommodate this complexity, but in a slightly different way for FEFF8 and WIEN2k.

TkATOMS produces only five unique potentials from the pentlandite unit cell parameters, two for metal sites, two for S sites and one for the selected absorbing atom. Before this can be used as an input file for $(Ni,Fe)_9S_8$ for FEFF8, two additional potentials must be added, with the appropriate associated stoichiometry, for the second metal atom (Ni or Fe) in tetrahedral and octahedral sites. For example, to model a pentlandite containing an equal proportion of Ni and Fe, the tetrahedral and octahedral site Ni and Fe potentials had to be assigned stoichiometries of 16 and 2, respectively. Additionally, in the list of ~250 metal atoms in the ~450 atom cluster generated by TkATOMS and radiating out from the absorbing atom, half of the atomic sites of each coordination had to be assigned to Ni and half to Fe, as only undifferentiated metal atom sites appear in the atoms list. This manual assignment must be done systematically for both the octahedral and tetrahedral sites to ensure the dispersal of each metal is as even as possible to model a random distribution. Calculations for

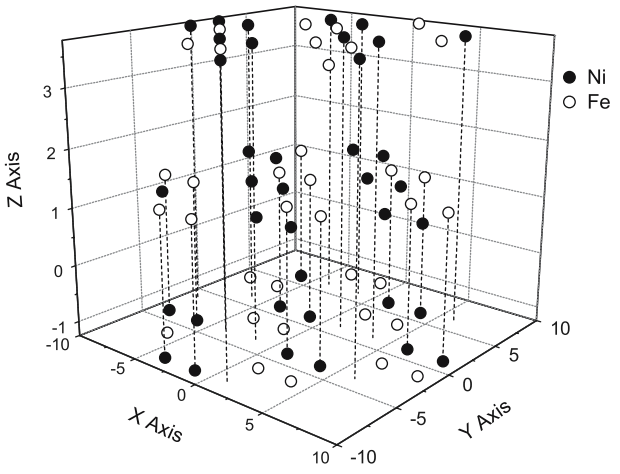


**Fig. 7** Pentlandite tetrahedral metal site cluster for FEFF8 input file showing an evenly distributed allocation of Ni and Fe atoms

**Table 2** Binding energies or binding energy differences calculated using FEFF8 or WIEN2k for the two S sites in (Fe,Ni) and Co pentlandites

| Mineral | S atom and coordination | Calculated binding energy or difference (eV) | | | |
|---|---|---|---|---|---|
| | | S 1*s* (FEFF8) | Δ[S 1*s*][a] (FEFF8) | Δ[S 1*s*] (WIEN2k) | Δ[S 2*p*] (WIEN2k) |
| $Ni_{4.5}Fe_{4.5}S_8$ | S1 [4] | 2469.85 | | | |
| | | | 0.31 | 0.52 | 0.49 |
| $Ni_{4.5}Fe_{4.5}S_8$ | S2 [5] | 2470.04 | | | |
| $Ni_5Fe_4S_8$ | S1 [4] | – | – | | |
| | | | | 0.51 | 0.46 |
| $Ni_5Fe_4S_8$ | S2 [5] | – | – | | |
| $Ni_4Fe_5S_8$ | S1 [4] | – | – | | |
| | | | | 0.48 | 0.43 |
| $Ni_4Fe_5S_8$ | S2 [5] | – | – | | |
| $Ni_9S_8$ | S1 [4] | 2469.65 | | | |
| | | | 0.24 | 0.51 | 0.46 |
| $Ni_9S_8$ | S2 [5] | 2469.8 | | | |
| $Fe_9S_8$ | S1 [4] | 2470.15 | | | |
| | | | 0.30 | 0.28 | 0.23 |
| $Fe_9S_8$ | S2 [5] | 2470.35 | | | |
| $Co_9S_8$ | S1 [4] | 2469.9 | | | |
| | | | 0.16 | 0.45 | 0.41 |
| $Co_9S_8$ | S2 [5] | 2470.1 | | | |

[a]Taking into account the small difference in the calculated Fermi level for the two calculations

four such arrangements, one of which is illustrated in Fig. 7 for tetrahedral sites, resulted in only minor differences, and representative values are listed for $Ni_{4.5}Fe_{4.5}S_8$ in Table 2.

For WIEN2k calculations, the unit cell parameters must be entered into the structure generation subroutine. The symmetry operations for the pentlandite structure were generated initially for the same element in all metal sites. When half these sites were assigned manually to Ni and half to Fe, the symmetry was no longer cubic, with the particular space-group transformation depending on which sites had been assigned to a particular metal. Only those transformations that did not change the nearest-neighbour distances were accepted, apart from that for $Ni_{4.5}Fe_{4.5}S_8$ for which the nearest-neighbour distances were altered slightly. WIEN2k calculations for several different stoichiometries were carried out and the binding energy differences for the two sites listed in Table 2. The preference by Fe atoms for octahedral sites deduced from Mössbauer spectra was accommodated by assuming a stoichiometry of $Ni_4Fe_5S_8$ with Fe atoms in all four octahedral sites in the unit cell. Calculations for $Ni_5Fe_4S_8$ could only be achieved by artificially assigning Ni atoms to all octahedral sites. The calculations for $Co_9S_8$ were carried out using the cell parameters for that material rather than for $(Ni,Fe)_9S_8$.

It can be seen from the data listed in Table 2 that the S 1*s* binding energies for pentlandite calculated by FEFF8 are in good agreement with the experimental S K-edge NEXAFS spectrum in Fig. 6a. It can also be seen that both codes indicate measurable S core electron binding energy differences for the 4- and 5-coordinate S atoms, and that for most stoichiometries, the energy difference calculated using FEFF8 is significantly less than that obtained with WIEN2k. In all cases, the calculated S 1*s* and S 2*p* binding energy differences were less than 0.55 and 0.5 eV, respectively, findings consistent with the S K-edge absorption and S 2*p* photoelectron spectra. In all cases, the calculated binding energy for the 5-coordinate S was greater than that for the 4-coordinate S, in agreement with the general relationship proposed on the basis of the pentlandite XPS studies by Legrand et al. (1997).

## Calculated densities of unfilled states and simulated NEXAFS spectra

The densities of unfilled states and simulated S K-edge NEXAFS spectra for pentlandite were calculated to assess any contribution to the S K-edge linewidth from the energy distribution of S *p*-states (as noted above), and to assess the S 1*s* binding energy difference needed for an acceptable simulation of the experimental S K-edge spectrum. Calculations using both FEFF8 and WIEN2k were carried out starting with the various stoichiometries and hence input files described in the previous section. First, in order to evaluate how well the calculated densities of unfilled states were able to rationalise the observed data, the S K-edge spectra simulated using FEFF8 and WIEN2k were compared with the experimentally determined spectra for pentlandite and heazlewoodite (Fig. 6). It is clear from Fig. 6 that both codes are able to simulate the experimental spectrum reasonably well. Therefore, the density of S *p*-states calculated by both codes (Fig. 8) should be a fair representation of the true density of states.

The region of the density of unfilled S *p*-states of relevance to the width of the leading absorption peak in

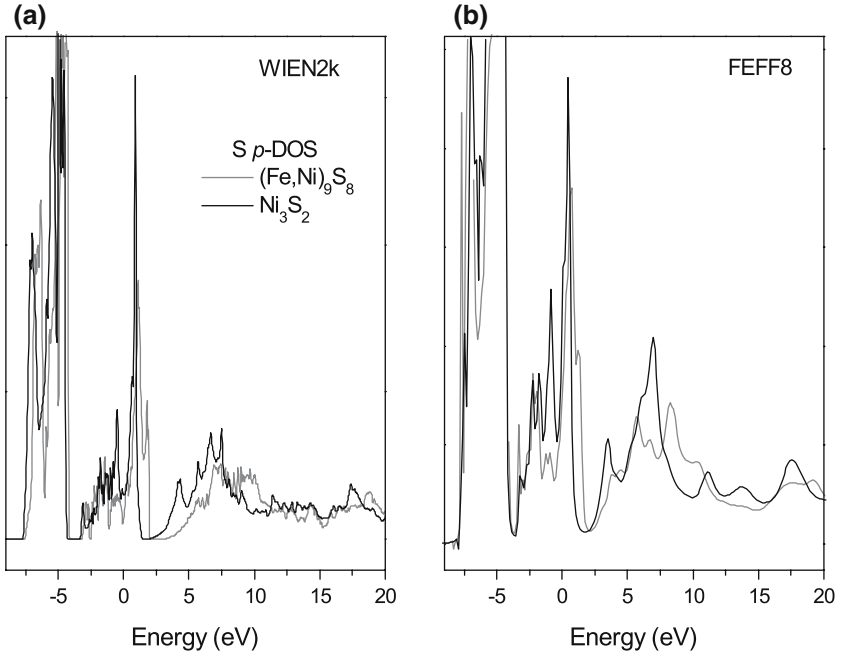


**Fig. 8** Densities of S *p*-states for pentlandite and heazlewoodite calculated using: **a** WIEN2k; **b** FEFF8

the S K-edge NEXAFS spectrum is the ~2 eV immediately above the Fermi level, in that the sooner the density falls to a low level after the Fermi level, the smaller the contribution to the width of the absorption peak will be. The density of S *p*-states calculated by both FEFF8 and WIEN2k for heazlewoodite falls to near zero at a lower energy than the corresponding density of states for pentlandite (Fig. 8). It is to be noted that the density of *p*-states is quite similar for both S sites in pentlandite, so that any difference in S 1*s* binding energy for the two sites will be reflected in the width of the S K-edge leading absorption peak, and not be compensated for by a similar energy shift in the distribution of unfilled states.

Thus, the calculations indicate that at least some of the broadening of the leading peak in the S K-edge NEXAFS spectrum for pentlandite arises from the form of the density of unfilled states. Hence not all the observed broadening would be due to a difference in the 1*s* binding energy for S atoms in 4- and 5-coordination. Indeed, the WIEN2k as-calculated binding energy difference appears to simulate the experimental S K-edge leading absorption peak quite well. On the other hand, an imposed increase of the S 1*s* binding energy difference to 0.9 eV (equivalent to a S 2*p* binding energy difference of 0.75 eV) would give rise to a noticeable asymmetry or incipient shoulder on the absorption edge, as illustrated in Fig. 9. The simulated S K-edge absorption spectra, then, are also consistent with a S 2*p* binding energy difference of less than 0.5 eV.

## Stibnite S 2*p* binding energies

The S 2*p* spectrum from an (010) surface prepared by fracture under UHV of a high-purity, natural specimen of the ~1.7 eV band-gap semiconductor stibnite determined at an instrumental resolution of about 0.35 eV and with charge 'neutralisation' was found to be a single symmetric doublet with $2p_{3/2}$ linewidth of 0.63 eV (Zakaznova-Herzog et al. 2006). The position of this spectrum, relative to a C 1s binding energy of 285 eV, was in excellent agreement with that obtained for synthetic $Sb_2S_3$ by Grigas et al. (2002), but the resolution of the S 2*p* doublet in the earlier study was poorer. The better-resolved spectrum was fitted more satisfactorily with three components each of linewidth 0.52 eV, equal intensity and separated by 0.2 eV corresponding to the 3 S sites in the stibnite structure than with a single component (Zakaznova-Herzog et al. 2006). An ab initio molecular orbital calculation had determined that the three non-equivalent S atoms had net charges of −0.46, −0.51 and −0.62 (Grigas et al. 2002), and as expected Zakaznova-Herzog et al. (2006) assigned the lowest binding energy component to the most negative S atom (S3). Assuming the validity of the fitting of the S 2*p* spectrum for stibnite, the two 3-coordinate S atoms have a 2*p* binding energy that differs by 0.2 eV, and the increase in S coordination number from 2 to 3 gives rise to a binding energy increase of an additional 0.2 eV, or an average value of ~0.3 eV. This difference is considerably less than the 0.8 eV difference postulated for 4- and 5-coordinate S in pentlandite (Legrand et al. 1997, 2005), but closer to the negligible binding energy difference observed for α- and β-NiS (Goh et al. 2006a). The stibnite data provide further evidence that a unit increase in S coordination does not necessarily lead to an increase in S 2*p* binding energy of ~0.8 eV as previously believed (Schaufuß et al. 1998).

In order to obtain an estimate of the binding energy difference for the three S atoms in stibnite, and to confirm that S atoms with the lower coordination corresponded to the lowest calculated binding energy, FEFF8 calculations of S 1*s* and S $2p_{3/2}$ binding energies, and WIEN2k calculations of S 2*p* binding energy differences, were carried out using the stibnite crystal lattice parameters of Kyono et al. (2002) (Table 3).

It is clear from the FEFF8-calculated binding energies listed in Table 3 that the 2-coordinate S is indeed expected to have a lower observed binding energy than either of the 3-coordinate S atoms. However, it is also clear from the binding energy differences calculated using WIEN2k, that any experimentally observed binding energy shifts would be small, and probably not greater than 0.1 eV. The fitted binding energy differences of 0.2–0.3 eV are slightly larger than expected from the calculations, but even if correct, are considerably smaller than might have been expected based on the previously postulated fitting of the pentlandite S 2*p* spectrum.

Apart from the similar 1*s* and 2*p* binding energies observed for the 5-coordinate S in β-NiS and the 6-coordinate S in α-NiS (Goh et al. 2006a), and the 2*p* binding energies for the 2- and 3-coordinate S in $Sb_2S_3$ differing by only ~0.3 eV (Zakaznova-Herzog et al. 2006), the results for pentlandite presented above add to the increasing experimental evidence that the core

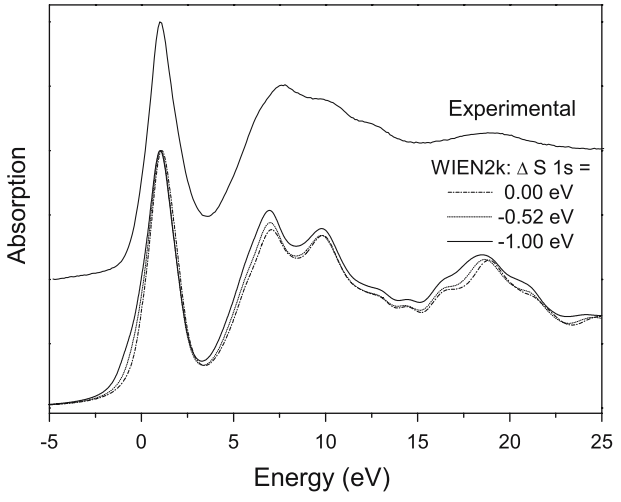


**Fig. 9** Observed S K-edge NEXAFS spectrum for pentlandite compared with spectra simulated using WIEN2k with imposed S 1*s* binding energy differences

**Table 3** 1*s* and 2*p* binding energies calculated by FEFF8, and 2*p* binding energy differences calculated by WIEN2k, for the 2- and 3-coordinate S atoms in stibnite

| S atom | Coordination | Fitted binding energy (eV) | Calculated binding energy or difference (eV) | | |
|---|---|---|---|---|---|
| | | | S 1*s* (FEFF8) | S 2*p* (FEFF8) | Δ[S 2*p*] (WIEN2k) |
| S1 | 3 | 162.2 | 2468.46 | 159.51 | |
| | | | | | 0.08 |
| S2 | 3 | 162.0 | 2468.46 | 159.51 | |
| | | | | | 0.05 |
| S3 | 2 | 161.8 | 2468.44 | 159.49 | |

electron binding energies for S vary less with coordination number than previously believed. It is true that the two S environments in covellite (CuS) have 2*p* binding energies that differ by 0.8 eV (Laajalehto et al. 1996), however those two environments are disulfide and monosulfide (Evans and Konnert 1976) rather than monosulfide in two different coordinations.

## Conclusion

The component near 161.4 eV in the S 2*p* photoelectron spectra from pentlandite surfaces freshly abraded in air under ambient conditions can be explained by the presence of the oxidation product violarite, which has a $2p_{3/2}$ binding energy near that value. The S 2*p* photoelectron spectra, S K-edge NEXAFS spectra, simulated S K-edge spectra and calculated S core electron binding energies were all consistent with a 2*p* binding energy difference for the 4- and 5-coordinate S in pentlandite being less than 0.5 eV, which is a smaller binding energy difference than previously proposed. The calculations did confirm, however, that the 5-coordinate S would have measurably larger core electron binding energies than the 4-coordinate S, in agreement with the earlier hypothesis. Calculations also confirmed that the 2*p* binding energy for the 3-coordinate S in stibnite would be higher than for the 2-coordinate, but that the binding energy difference was quite small, in accord with the S 2*p* photoelectron spectrum for that mineral. Therefore, in interpreting S 2*p* spectra for other sulfide minerals, it should not be argued that a unit increase in coordination gives rise to a binding energy increase of ~0.8 eV, or even that the binding energy increase will necessarily be significant.

**Acknowledgements** This work was supported by the Australian Synchrotron Research Program, which is funded by the Commonwealth of Australia under the Major National Research Facilities Program. The authors are grateful to Dr. D. Moran for assistance in carrying out large-cluster FEFF8 calculations on a supercomputer available through the Australian Partnership for Advanced Computing National Facility, to Prof. P. Blaha, for advice on using WIEN2k, and to Dr. V. Keast, for guidance in handing the WIEN2k input file for pentlandite. The authors are also grateful for assistance with computing by H. S. Chan and with operation of XPS equipment by Dr. B. Gong. Pentlandite specimens were supplied by Dr. D. French, and the synthetic heazlewoodite was provided by Prof. R. Woods. Dr. M. Kasrai and Prof. A. Gerson kindly provided pentlandite S K-edge spectra for comparison with data collected in the present work.

## References

Ankudinov AL, Ravel B, Rehr JJ, Conradson SD (1998) Real-space multiple-scattering calculation and interpretation of X-ray-absorption near-edge structure. Phys Rev B 58:7565–7576

Ankudinov AL, Bouldin CE, Rehr JJ, Sims J, Hung H (2002) Parallel calculation of electron multiple scattering using Lanczos algorithms. Phys Rev B 65:104107-1–104107-11

Blaha P, Schwarz K, Sorantin P, Trickey SB (1990) Full-potential, linearized augmented plane wave programs for crystalline systems. Comput Phys Commun 59:399–415

Buckley AN, Woods R (1985) X-ray photoelectron spectroscopy of oxidized pyrrhotite surfaces. I. Exposure to air. Appl Surf Sci 22/23:280–287

Buckley AN, Woods R (1991a) Surface composition of pentlandite under flotation-related conditions. Surf Interface Anal 17:675–680

Buckley AN, Woods R (1991b) Electrochemical and XPS studies of the surface oxidation of synthetic heazlewoodite ($Ni_3S_2$). J Appl Electrochem 21:575–582

Chassé T, Peisert H, Streubel P, Szargan R, Meisel A (1993) XPS binding energies of deep core levels and the Auger parameter—an application to solid sulfur compounds. Acta Phys Pol A 83:793–802

Chauke HR, Nguyen-Manh D, Ngoepe PE, Pettifor DG, Frioes SG (2002) Electronic structure and stability of the pentlandites $Co_9S_8$ and $(Fe,Ni)_9S_8$. Phys Rev B 66:155105-1–155105-5

Evans HT Jr, Konnert JA (1976) Crystal structure refinement of covellite. Am Mineral 61:996–1000

Fleet ME (1977) The crystal structure of heazlewoodite, and metallic bonds in sulfide minerals. Am Mineral 62:341–345

Francis CA, Fleet ME, Misra K, Craig JR (1976) Orientation of exsolved pentlandite in natural and synthetic nickeliferous pyrrhotite. Am Mineral 61:913–920

Goh SW, Buckley AN, Lamb RN, Skinner WM, Pring A, Wang H, Fan L-J, Jang L-Y, Lai L-J, Yang Y-w (2006a) Sulfur electronic environments in α-NiS and β-NiS: examination of the relationship between coordination number and core electron binding energies. Phys Chem Minerals 33:98–105

Goh SW, Buckley AN, Lamb RN, Rosenberg RA, Moran D (2006b) The oxidation states of copper and iron in mineral sulfides, and the oxides formed on initial exposure of chalcopyrite and bornite to air. Geochim Cosmochim Acta 70:2210–2228

Grigas J, Talik E, Lazauskas V (2002) X-ray photoelectron spectroscopy of $Sb_2S_3$ crystals. Phase Transit 75:323–337

Knipe SW, Mycroft JR, Pratt AR, Nesbitt HW, Bancroft GM (1995) X-ray photoelectron spectroscopic study of water adsorption on iron sulphide minerals. Geochim Cosmochim Acta 59:1079–1090

Knop O, Huang C-H, Woodhams FWD (1970) Chalcogenides of the transition elements. VII. A Mössbauer study of pentlandite. Am Mineral 55:1115–1130

Krause MO, Oliver JH (1979) Natural widths of atomic *K* and *L* levels, *Kα* X-ray lines and several *KLL* Auger lines. J Phys Chem Ref Data 8:329–338

Kwok RWM (2000) XPSPEAK version 4.1; freeware

Kyono A, Kimata M, Matsuhisa M, Miyashita Y, Okamoto K (2002) Low-temperature crystal structures of stibnite implying orbital overlap of Sb $5s^2$ inert pair electrons. Phys Chem Minerals 29:254–260

Laajalehto K, Kartio I, Kaurila T, Laiho T, Suoninen E (1996) Investigation of copper sulfide surfaces using synchrotron radiation excited photoemission spectroscopy. In: Mathieu HJ, Reihl B, Briggs D (eds) Proc ECASIA '95, Wiley, Chichester, pp 717–720

Legrand DL, Bancroft GM, Nesbitt HW (1997) Surface characterization of pentlandite, $(Fe,Ni)_9S_8$, by X-ray photoelectron spectroscopy. Int J Miner Process 51:217–228

Legrand DL, Bancroft GM, Nesbitt HW (2005) Oxidation/alteration of pentlandite and pyrrhotite surfaces at pH 9.3: Part 1. Am Mineral 90:1042–1054

Li D, Bancroft GM, Kasrai M, Fleet ME, Feng X, Tan K (1995) S K- and L-edge X-ray absorption spectroscopy of metal sulfides and sulfates: applications in mineralogy and geochemistry. Can Mineral 33:949–960

Misra KC, Fleet ME (1974) Chemical composition and stability of violarite. Econ Geol 69:391–403

Pearson AD, Buerger MJ (1956) Confirmation of the crystal structure of pentlandite. Am Mineral 41:804

Rajamani V, Prewitt CT (1973) Crystal chemistry of natural pentlandites. Can Mineral 12:178–187

Ravel B (2001) *ATOMS*: crystallography for the X-ray absorption spectroscopist. J Synchrotron Radiat 8:314–316

Richardson S, Vaughan DJ (1989) Surface alteration of pentlandite and spectroscopic evidence for secondary violarite formation. Mineral Mag 53:213–222

Schaufuß AG, Nesbitt HW, Kartio I, Laajalehto K, Bancroft GM, Szargan R (1998) Incipient oxidation of fractured pyrite surfaces in air. J Electron Spectrosc 96:69–82

Schwarz K, Blaha P, Madsen GKH (2002) Electronic structure calculations of solids using the WIEN2k package for material sciences. Comput Phys Commun 147:71–76

Sodhi RNS, Cavell RG (1986) *KLL* Auger and core level (1*s* and 2*p*) photoelectron shifts in a series of gaseous sulfur compounds. J Electron Spectrosc 41:1–24

Vaughan DJ, Ridout MS (1971) Mössbauer studies of some sulphide minerals. J Inorg Nucl Chem 33:741–746

Zakaznova-Herzog VP, Harmer SL, Nesbitt HW, Bancroft GM, Flemming R, Pratt AR (2006) High resolution XPS study of the large-band-gap semiconductor stibnite ($Sb_2S_3$): structural contributions and surface reconstruction. Surf Sci 600:348–356